Originally Published at ISTFA 2022: Proceedings from the 48th International Symposium for Testing and Failure Analysis Conference

Seeing beyond

A Correlative Microscopic Workflow For Nanoscale Failure Analysis and Characterization of Advanced Electronics Packages

Thomas Rodgers, Allen Gu, Greg Johnson, Masako Terada, Nathaniel Cohan, Vignesh Viswanathan
Carl Zeiss Microscopy GmbH, Carl-Zeiss Strasse 22, 73447 Oberkochen, Germany

Michael W. Phaneuf, Joachim de Fourestier, Ethan Ruttan
Fibics Inc., 1431 Merivale Rd #100, Ottawa, ON K2E 0B9, Canada

Stewart McCracken, Suzanne Costello, Aidan M Robinson, Andrew Gibson, Alan Balfour
Materials Consultancy Services Limited, Centre House, Midlothian Innovation Centre, Roslin, Midlothian, EH25 9RE, United Kingdom

Abstract

Microscopic imaging and characterization of semiconductor devices and material properties often begin with a sample preparation step. A variety of sample preparation methods such as mechanical lapping and broad ion beam (BIB) milling have been widely used in physical failure analysis (FPA) workflows, allowing internal defects to be analyzed with high-resolution scanning electron microscopy (SEM). However, these traditional methods become less effective for more complicated semiconductor devices, because the cross-sectioning accuracy and reliability do not satisfy the need to inspect nanometer scale structures. Recent trends on multi-chip stacking and heterogenous integration exacerbate the ineffectiveness. Additionally, the surface prepared by these methods are not sufficient for high-resolution imaging, often resulting in distorted sample information. In this work, we report a novel correlative workflow to improve the cross-sectioning accuracy and generate distortion-free surface for SEM analysis. Several semiconductor samples were imaged with 3D X-ray microscopy (XRM) in a non-destructive manner, yielding volumetric data for users to visualize and navigate at submicron accuracy in three dimensions. With the XRM data to serve as 3D maps of true package structures, the possibility to miss or destroy the fault regions is largely eliminated in PFA workflows. In addition to the correlative workflow, we will also demonstrate a proprietary micromachining process which is capable of preparing deformation-free surfaces for SEM analysis.

Introduction

As semiconductor package architectures become more complex, the schemes of heterogeneous integration provide greater complexity in dimensions, density, and delicacy of IC interconnects. The diagnosis methods of encapsulated structures and failures are under increasing demands. One challenge is to isolate and pinpoint fault regions with sufficient accuracy during the PFA process.

Because typical modern ICs are made of a variety of materials with different coefficients of thermal expansion (CTE), warpages exist ubiquitously in die, package, and PCB levels, resulting in significant positional shifts of the structures respective to IC designs. If the original design is used to guide cross-section, it may yield wrong surfaces, possibly losing defects or regions of interest permanently. The capability to acquire true 3D reconstruction of failure locations becomes crucial for the success of root cause analysis. Although the conventional mechanical lapping and BIB milling are effective to remove materials from large areas, it is not accurate because there is limited control at endpoint. Modern advanced packages are often made of various materials in silicon, metals, and organic polymers with length scales ranging from millimeters to nanometers. This dynamic provides additional challenges to the existing sample preparation and PFA workflows.

3D X-ray tomography has become an essential technique for construction and failure analysis of semiconductor packages [1-4]. Its non-destructive nature and high-resolution imaging capability make it an ideal tool to reconstruct package structures with high resolution. With the assistance of acquired 3D XRM datasets, analysts can virtually navigate through an entire package volume to identify specific regions of the interest and characterize failures. This makes the subsequent cross-sections more effective than xconventional polishing. Recently, we have demonstrated that the integration of laser ablation with focused ion beam (FIB) techniques for fine polishing has enabled rapid preparation of site-specific cross-sections with extremely high precision [5-6]. In this paper, we report a three-step PFA process dedicated to preparing SEM surface with high accuracy and pristine quality. Firstly, a semiconductor package is imaged with high-resolution 3D XRM, and regions of interest are defined at submicron accuracy. Secondly, using the acquired 3D X-ray data, a proprietary sample cross-sectioning process Perfect Edge [7] follows to generate accurate and distortion-free surfaces. Thirdly, the prepared surface is imaged and analyzed with FE-SEM.

Copyright 2022 ASM International All rights reserved. www.asminternational.org

Results

SiP Wire Bonds

A commercially available ADAQ23875 system-in-package (SiP) device was purchased using a standard commercial channel. The sample was overstressed with excessive current provided by a Keithley probe station. The test stopped when 100X decrease in current was observed in I-V curves. The sample then was imaged by 3D X-ray microscopy at 10 µm/voxel resolution to capture full field of view (FOV) of the package. 120 kV X-ray energy was used to image this medium density sample. A high-resolution image at 1.5 µm/voxel was acquired. Figure 1 shows the 3D color-rendering image and examples of reconstructed virtual slices.

The XRM data was processed using analysis workflows within ORS Dragonfly to "digitally" remove encapsulating packaging material and reveal the internal components of the SiP, including the gold wire bonds, ICs, passive components, and the underlying PCB substrate. In Figure 2, specific electric networks of interest with the suspicion of partial wire opening (associated with excessive resistance) are labeled on the planar views of the XRM images. The flexibility of 3D digital data manipulation makes it easy to visualize the internal structures at any orientation.

Having selected a wire bond arc of interest (the primary target wire bond #1 in Figure 3), the sample was then cross-sectioned using the propriety Perfect Edge process which combines a mechanical cutting step and inert gas plasma polishing. This process flow was developed to enable key micro-structural information to be extracted from samples with speed and accuracy, allowing us to target features within packages such as the SiP package studied here. Because the X-ray images provide excellent interior 3D information, there is no need for de-encapsulation prior to the physical cross-section. The process allows us to minimize artifacts, optimize preparation process, and increase positioning accuracy, making it possible to reliably target features with the accuracy down to submicron. Figure 4 shows the cross-section SEM image of the target Au wire with the assistance of the XRM image (Figure 4 top). The entire gold wire loop is accurately sectioned and undamaged between ball and wedge bonds.

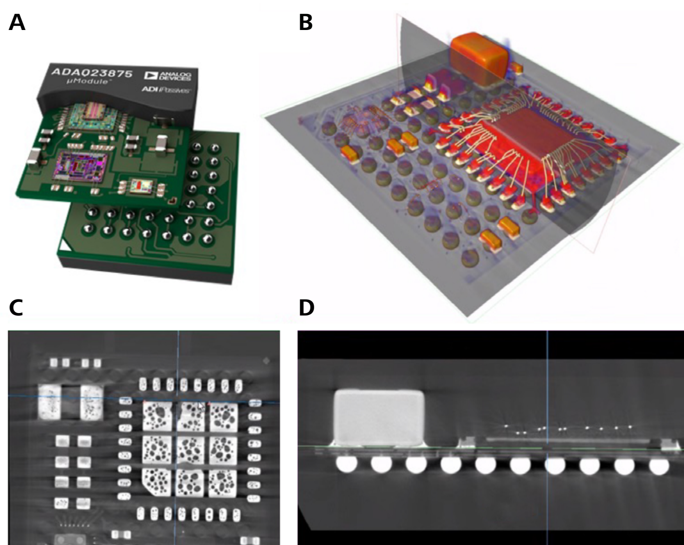

Figure 1 3D X-ray tomography compared to schematic. A) Schematics of dissected SiP (marketing material) suggest the internal chips and electric net design. B) 3D color-rendering of acquired tomography shows internal wire bond networks in this study. C-D) examples of virtual cross-sections.

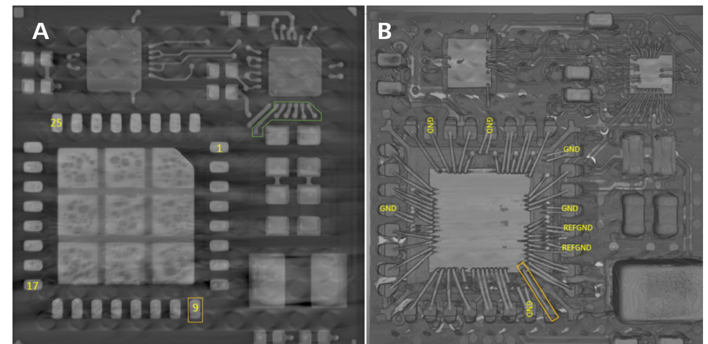

Figure 2 The electric networks of interest with the suspicion of partial open (high resistance) are labeled on the planar views of 3D XRM images: A) bottom side view of the ADC (LTC2387-16). B) top side view.

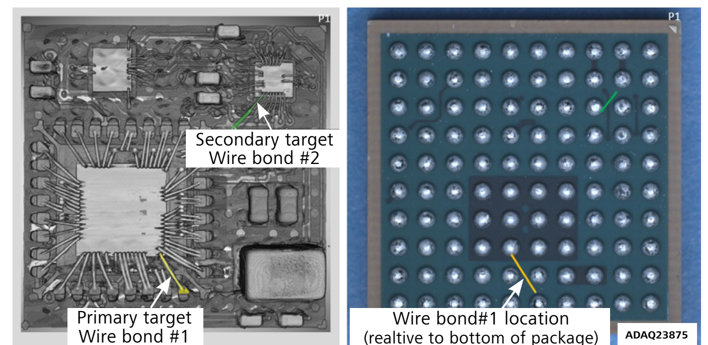

Figure 3 Two target leads (labeled as yellow and green) were chosen in this study for demonstration purpose. The wire bonds lie at an oblique angle to the edge of the package. The photo on the right shows the positions of these two wires on an optical image.

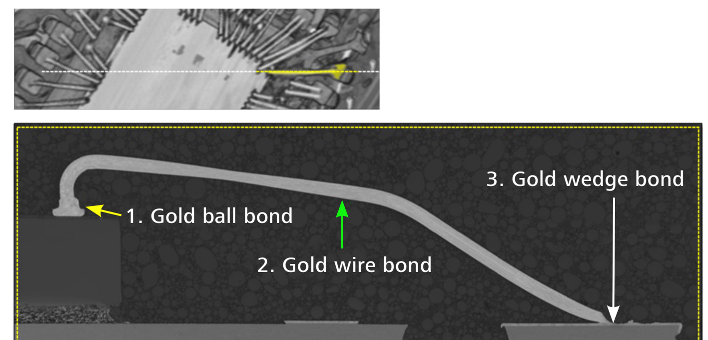

Figure 4 An XRM virtual cross-section (top) and SEM image (below) show the entire targeted wire bond. The sample was analyzed to confirm the condition of electrical connectivity. The gold wire loop is undamaged between ball and wedge bonds.

Copyright 2022 ASM International All rights reserved. www.asminternational.org

Because the Perfect Edge process provides a large surface free of contamination and distortion, we are able to acquire high-quality SEM images which reflect unaltered sample conditions. Figure 5 shows the ball bond made between gold wire and aluminum bond pad on the die. The moulded component body, wire bond and die are all clearly visible. Figure 6 shows that several phases of the intermetallic compounds (IMCs) were formed at the interface of the gold ball and the aluminum pad. IMCs provide physical and electrical connection between the wire and die. These IMC phases were further analzyed by Energy Dispersive Spectroscopy (EDS) in Figure 7. A thin layer of aluminum oxide (blue arrows in Figure 6-7) was formed between two IMC phases. A high-magnification image further confirms the oxide-rich region in Figure 8. We believe that this oxide layer could be the root cause of the excessive resistance observed during the overstress test, which is consistent to the report [6]. A further investigation is required to confirm that the oxide growth is responsible to the high resistance of the Au wire loop. As the main topic of this work is to develop the correlative sample preparation and imaging workflow, we continue to focus on the workflow.

HBM-Interposer Microbumps

A drawback of physical failure analysis is that the success rate strongly depends on how precisely the upstream non-destructive techniques can isolate and pinpoint the fault locations. Without accurate 3D geographic information, a failure region may be destroyed or altered during the PFA process, leading to no arrival of root causes. On a second case study, we choose an AMD Vega 64 2.5D interposer package as the test vehicle due to its multi-chip 3D stacks and large area (50 x 50 mm) silicon interposer connected with HBM using 20 μm Cu pillars and small volume solders. The complexity of the IC architecture challenges the conventional PFA workflows.

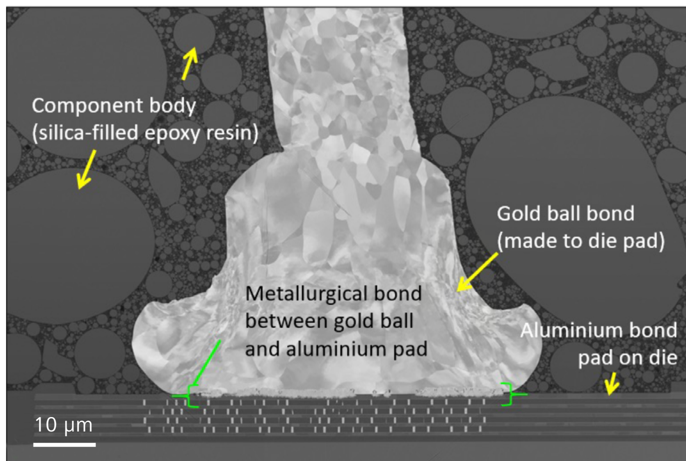

Figure 5 *Ball bond made between gold wire and aluminum bond pad. The moulded component, wire bond and die are all clearly visible. A metallurgical bond was formed between the gold and the aluminum during device manufacturing. This provides physical and electrical connection between the wire and die.*

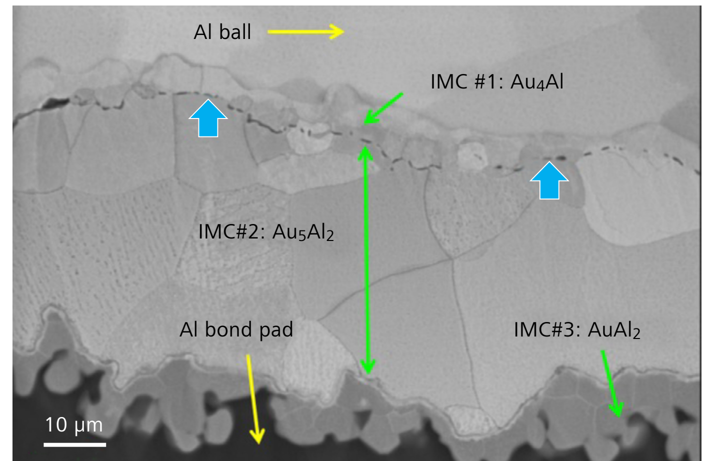

Figure 7 *Ball bond made between gold wire and aluminum bond pad. Several Au-Al IMC phases have formed. Energy Dispersive X-ray (EDS) analysis was used to identify the IMC phases (labelled here for reference).*

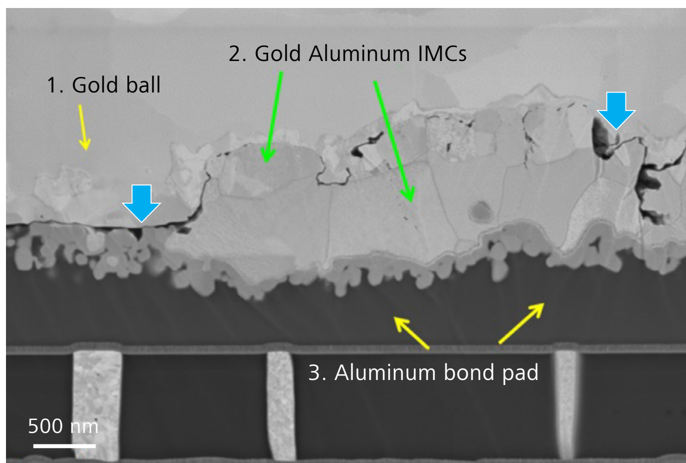

Figure 6 *Ball bond between gold wire and aluminum bond pad. Several Au-Al intermetallic compounds (IMC) phases have formed. IMCs can change over time in response to elevated temperature (solid-state diffusion). In severe cases, solid-state changes can cause de-bonding and bond failure.*

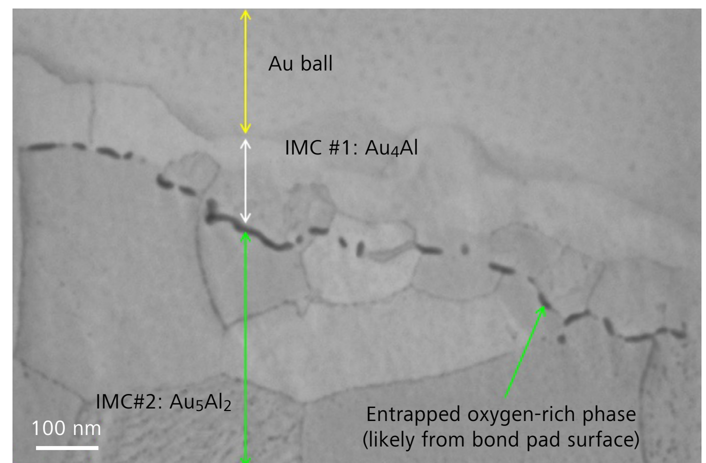

Figure 8 *Part of a ball bond made between gold wire and aluminum bond pad. Two Au-Al IMC phases have formed with a thin layer of oxygen-rich material between the two IMC phases.*

Copyright 2022 ASM International All rights reserved. www.asminternational.org

3D X-ray data was acquired with 90 kV energy at 0.7 µm/voxel resolution for the 2.5D package using XRM 4X optical objective. The fault region was microbump joint cracks at the interposer interface formed during thermal compression bonding process. The X-ray data clearly shows ~2 µm thick bump cracks in all three orientations (Figure 9b-d). With the information of the defect location in 3D to facilitate the sample preparation, physical cross-sectioning and SEM analysis followed to investigate possible root causes of the joint cracks. In this case, the Perfect Edge process was not employed. It is virtually impossible to do an accurate cross-section without the guidance of 3D X-ray data because the layer of the target microbumps are deeply buried, and therefore they are not visible by optical methods.

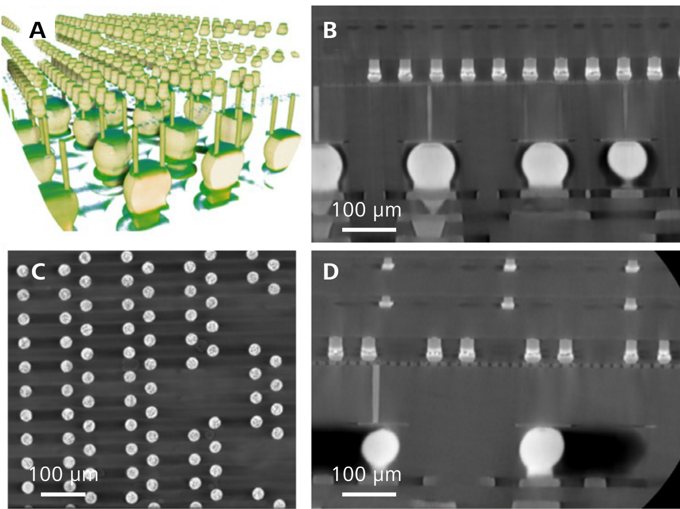

Figure 9 *3D X-ray tomographic images at 0.7µm/vox of the HBM 2.5D interposer package. A) 3D color-rendering image. B) Virtual slice shows the microbump layer between the Si interposer and HBM. C) planar view of the microbump layer. D) side view of the same layer of the microbumps.*

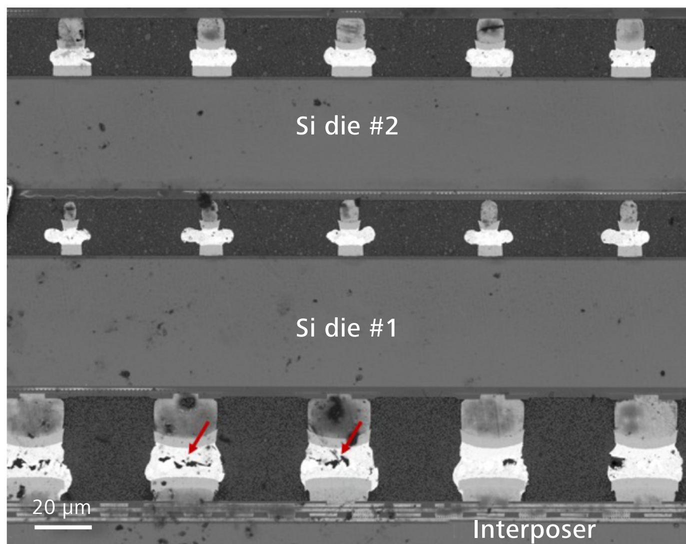

Figure 10 *Backscatter electron image of the microbump layer with two HBM die stacks on the top. The image was conducted with 5 kV acc. voltage at 86 nm/pixel.*

It is also not feasible to use the HBM bumps on the top layer as reference because they are not fully aligned with the target layer of microbumps in XY orientations (Figure 9d). To our best knowledge, XRM imaging is the only non-destructive technique which can reconstruct internal 3D structures of this package and provide sufficient resolution on the joint cracks.

Figure 10 shows a backscatter electron microscope image of the target bump layer at the bottom of the micrograph. Conducting imaging at 5 kV accelerating voltage in high vacuum using the pixel size of 86 nm, the microbump joint cracks (indicated by red arrows) are clearly visible during the sample cross-sectioning through the center of the target microbumps. This image validates the existence of µbump micro-cracks observed in 3D XRM images. Figure 11 shows an individual microbump with solder joint cracks. It seemed that Ni pad layers and Cu pillars were intact without any sign of failure. Several intermetallic compounds (IMCs) phases were observed on the target microbump (Figure 11b).

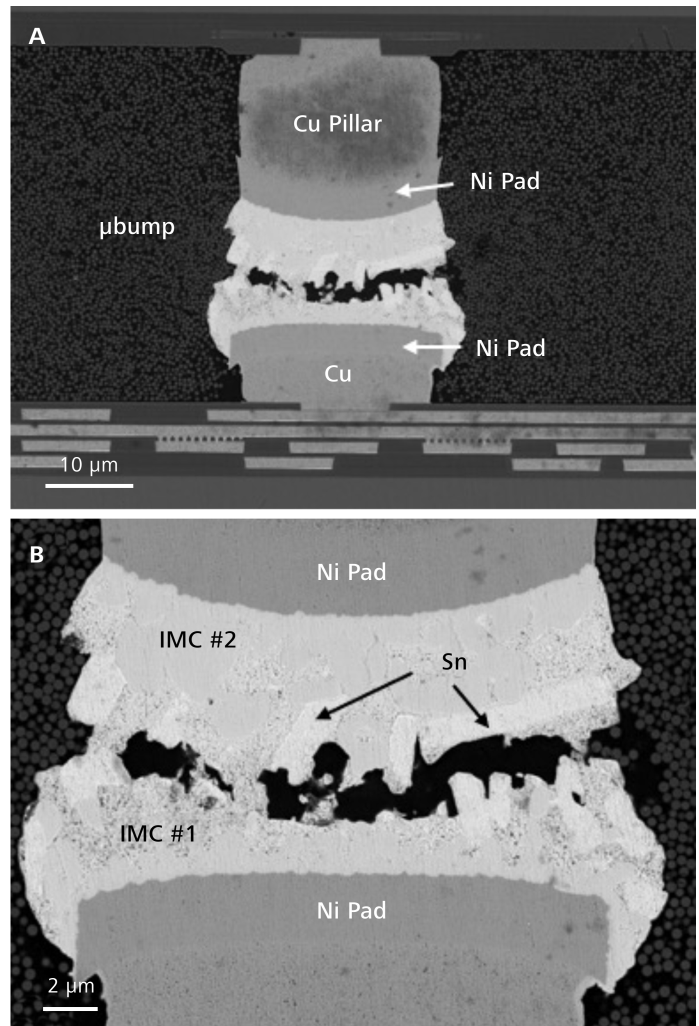

Figure 11 *Backscatter electron images of a microbump crack imaged at 5 kV acc. voltage with an annular backscatter detector. A) 37 nm/pixel; B) 15 nm/pixel.*

Copyright 2022 ASM International All rights reserved. www.asminternational.org

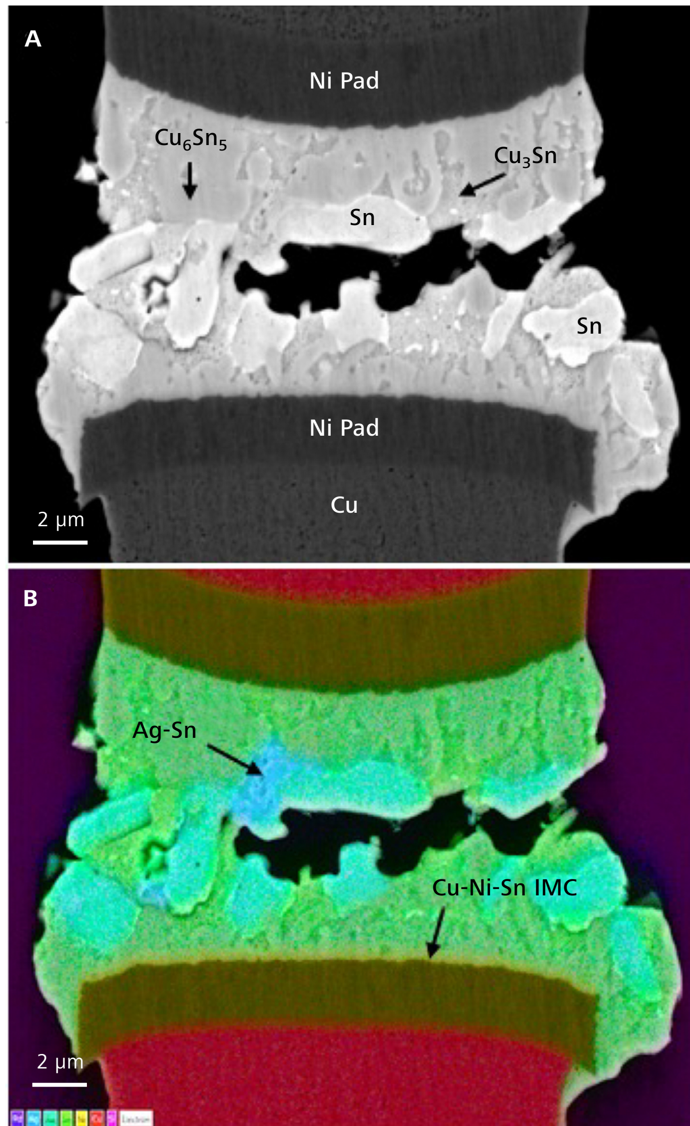

Figure 12 *Backscatter electron image and energy dispersive X-ray spectroscopy (EDS) elemental map of a cracked microbump with distinct metal phases in the solder and solder mask. The pixel size is 31 nm.*

The backscatter image in Figure 12a and the EDS elemental map image in Figure 12b show the cracked microbump with several metal phases in the solder materials. Analytical imaging conditions were 17 kV accelerating voltage with 3 nA beam current at a working distance of 8.5 mm, map live time 576 seconds using an EDS detector. We were able to identify the different IMC phases formed during thermal compression bonding assembly. Based on the X-ray data, SEM images, and EDS information on the bump metallurgy, we concluded that the large interposer warpage is likely to generate sufficient shear force on the microbump layer, leading to the crack formation and propagation. There was no other metallic abnormality observed in this case.

Conclusion

We demonstrated a correlative microscopic workflow that integrates XRM's non-destructive 3D imaging capability to PFA workflows, enabling analyzer to precisely locate and prepare defects of interest for nanoscale imaging and characterization with SEM. We investigated a wire bonding in a commercial SiP device and a microbump in a 2.5D interposer package to exemplify the microscopic workflow and the Perfect Edge process to prepare a pristine SEM surface. With more incoming challenges in effective defect isolation and localization for 3D packaging and heterogeneous integration, this workflow can be used to significantly improve the effectiveness of PFA workflows by providing highly accurate 3D information to guide the subsequent crosssections.

Copyright 2022 ASM International All rights reserved. www.asminternational.org

References

[1] L. Mirkarimi, A. Gu, L. Hunter, G. Guevara, M. Huynh, R. Katkar, "X-ray Microscopy and Root Cause Analysis in Electronic Packaging", *Proc 41st Int'l Symp for Testing and Failure Analysis,* Portland, OR, Nov. 2015, pp. 430-435. doi: 10.31399/asm.cp.istfa2015p0430

[2] A. Gu, A. Andreyev, M. Terada, B. Zee, S. M. Zulkifli, Y. Yang, "Accelerate Your 3D X-ray Failure Analysis by Deep Learning High Resolution Reconstruction Paper," Int'l Symp for Testing and Failure Analysis, No: istfa2021p0291, pp. 291-295, Phoenix, AZ, Dec 2021.

[3] S. M. Zulkifli, B. Zee, W. Qiu, A. Gu, "High-Res 3D X-ray Microscopy for Non-Destructive Failure Analysis of Chip-to-Chip Micro-bump Interconnects in Stacked Die Packages", *IEEE 24th Int'l Symp on the Physical and Failure Analysis of Integrated Circuits (IPFA),* Chengdu, China, Jul. 2017. doi:10.1109/IPFA.2017.8060111

[4] A. Gu, J. Auyoong, "3D Measurement Workflow for Packaging Development and Production Control Using High-Resolution 3D X-ray Microscope", *2018 IEEE 20th Electronics Packaging Tech Confer (EPTC),* Singapore, Dec. 2018. doi:10.1109/EPTC.2018.8654390

[5] Viswanathan and L. Jiao, "Developments in Advanced Packaging Failure Analysis using Correlated X-Ray Microscopy and LaserFIB," 2021 IEEE 23rd Electronics Packaging Technology Conference (EPTC), 2021, pp. 80-84, doi: 10.1109/EPTC53413.2021.9663938

[6] A. Gu, M. Terada, H. Stegmann, T. Rodgers, C. Fu and Y. Yang, "From System to Package to Interconnect: An Artificial Intelligence Powered 3D X-ray Imaging Solution for Semiconductor Package Structural Analysis and Correlative Microscopic Failure Analysis," IPFA 2022, Singapore

[7] Application Note, Materials Consultancy Services Ltd., Midlothian Innovation Centre, Midlothian, UK, 2020; https://www.themcsgroup.co.uk

[8] M. J. McCracken, "Assessing Au-Al Wire Bond Reliability Using Integrated Stress Sensors", MS thesis, University of Waterloo, Waterloo, Ontario, Canada, 2010

microscopy@zeiss.com
www.zeiss.com/semiconductor-microscopy

Copyright 2022 ASM International All rights reserved. www.asminternational.org

ISTFA 2022: Proceedings from the 48th International Symposium for Testing and Failure Analysis Conference